Cement and Concrete Research 41 (2011) 893–902

Contents lists available at ScienceDirect

Cement and Concrete Research

journal homepage: http://ees.elsevier.com/CEMCON/default.asp

Cover cracking of reinforced concrete due to rebar corrosion induced by chloride penetration

Santiago Guzmán [a], Jaime C. Gálvez [a,*], José M. Sancho [b]

[a] Departamento de Ingeniería Civil: Construcción, E.T.S. de Ingenieros de Caminos, Canales y Puertos, Universidad Politécnica de Madrid, C/ Profesor Aranguren s/n, 28040 Madrid, Spain
[b] Departamento de Estructuras de Edificación, E.T.S. Arquitectura, Av. Juan de Herrera 4, 28040 Madrid, Spain

ARTICLE INFO

Article history:
Received 5 October 2010
Accepted 15 April 2011

Keywords:
Chloride (D)
Diffusion (C)
Corrosion (C)
Cracking
Durability (C)

ABSTRACT

Cracking of concrete cover due to corrosion induced expansion of steel rebar is one of the major causes of the deterioration of reinforced concrete (RC) structures exposed to marine environments and de-icing salts.
This paper presents two models that deal with the chloride-induced corrosion and subsequent cracking of concrete cover in RC structures. The former analyses the chloride diffusion within partially saturated concrete. A comprehensive model is developed through the governing equations of moisture, heat and chloride-ion flow. Nonlinearity of diffusion coefficients, chloride binding isotherms and convection phenomena are also highlighted. The latter describes the internal cracking around the bar due to expansive pressures as corrosion of the reinforcing bar progresses. Once a certain chloride concentration threshold is reached in the area surrounding the bar, oxidation of steel begins and oxide products are generated, which occupy much greater volume than the original steel consumed by corrosion. An embedded cohesive crack model is applied for cracking simulation.
Both models are incorporated in the same finite element program. The models are chained, though not explicitly coupled, at first instance. Comparisons with experimental results are carried out, with reasonably good agreements being obtained. The work is a step forward for the integration of the two traditional phases (initiation and propagation) widely used in the literature and usually analysed separately. The estimation of the service life of the structure needs to evaluate the associated time for each one.

1. Introduction

Corrosion of reinforcement bars is a primary cause in the deterioration of concrete structures which may lead to failure and even collapse. In any case, the cost of the associated repair and maintenance is enormous (for example, Kirkpatrick et al. [1]). Chloride induced corrosion of the reinforcing steel is known to be a major cause of premature rehabilitation of reinforced concrete structures.

Hence, research relating to the durability assessment of concrete structures has shown a substantial increase in recent years. However, many factors involved in the chloride induced corrosion process remain poorly understood. In spite of significant progress in predicting models, the estimation of service life of reinforced concrete (RC) structures is yet to be satisfactorily defined.

Present work is focused on chloride attack and distinguishes the two distinct phases traditionally adopted in the literature [2]: the initiation stage, until aggressive species concentration around the reinforcement bar reaches a threshold value, necessary to trigger active corrosion; and the propagation stage, in which rust generation induces tensile stresses in the concrete cover. This work sets out to integrate the two phases (initiation and propagation) widely cited in the literature and usually analysed separately. An overview of the previous proposals leads the reader to the general conclusion that service life ends when steel depassivates (the initiation phase) [3]. In this work, the above models are chained though not explicitly coupled. On a first calculation the chloride ingress and transportation are studied. When the chloride concentration around the reinforcement bar reaches a threshold value, the concrete cracking cover is then examined, through the second model.

Depending on the scale, the modelling of the concrete can be performed with different levels of abstraction, from a detailed representation of the concrete components (aggregates, cement paste, voids, among others), based on a micro-modelling approach, to a global analysis as a continuum. This paper presents a meso-modelling procedure for analysis of the chloride ingress and transportation and concrete cracking. The model does not make any distinction among individual components of concrete, averaging the effect of the composite material through the formulation of a fictitious continuous material. The material is assumed to be homogeneous and isotropic. The meso-scale approach has been successful for chloride

* Corresponding author. Tel./fax: +34 913365350.
E-mail addresses: guzman.s@tecnicasreunidas.es (S. Guzmán), jaime.galvez@upm.es (J.C. Gálvez), jose.sancho@upm.es (J.M. Sancho).

0008-8846/$ – see front matter © 2011 Elsevier Ltd. All rights reserved.
doi:10.1016/j.cemconres.2011.04.008

ingress and transportation ([4–6], among others) and for concrete cracking [7–9].

With reference to the initiation stage, several mathematical models have been developed to describe the chloride ingress and transport into concrete. Although the former approaches have considered the transport of ions only under the effect of diffusion by the mere application of 2nd Fick's law, other phenomena such as convection (motion of dissolved substances caused by flow of water in pore solution of partially saturated media) or chloride binding (capacity of free chloride of being chemically bound, particularly with C_3A to form Friedel salts) are taken into account in a very simple way [10,11]. The electrical coupling between the ions in multiionic models is taken into account by Masi et al. [12], though in the framework of saturated concrete. Under a similar assumption, Barbarulo et al. [44] have used the activity coefficients of the species and even a non-instantaneous rate of dissolution/precipitation of the various species in the solution.

Here, a special purpose computer program was implemented by the authors. The approach is a single-ion model, considering only chloride and the effect of diffusion and convection. Given the ideal nature of the ionic solutions, activity effects can be neglected. The effect of chloride binding is introduced under local chemical equilibrium, valid except for cases where ions are transported very quickly through the material pore structure (for example, under an externally applied electrical potential). The chloride binding is not taken into account in the diffusion process by means of an apparent diffusion coefficient [6,13], but by developing the complete set of equations consisting of time-dependent such equations for both the chloride concentration within the pore solution and the moisture content within the pore space [14,15], by averaging the relevant microscopic transport equations over a representative volume element. Three macroscopic variables are used: chloride concentration, moisture and temperature.

Instead of other comprehensive models with combined effects of pore solution convection and ionic interaction though with constant ionic diffusion coefficients (for example, Wang et al. [16]), the approach here focuses attention on the interdependence between chloride and moisture flows, with variable diffusion coefficients [6,11], particularly for an ideal situation of ingress of chloride through one salt with a given type of cation.

Regarding the propagation stage, corrosion provokes the reinforcement cross-section reduction and loss of bond between concrete and steel. Moreover, oxide products occupy much greater volume than the original steel consumed [17,18]. Tensile stresses are generated in the surrounding concrete, resulting in cracking and, eventually, spalling and delamination (for example, Liu and Weyers [19]). The two Finite Element (FE) approaches traditionally used to simulate concrete cracking: smeared cracking and discrete cracking, have been successfully complemented in the last years by application of the so-called Strong Discontinuity Approach (SDA, [20]). Analytical implementation of the discrete crack model, based on the thick walled-cylinder approach, has been proposed (for example, Bhargava and Ghosh [21]), and even FE implementation of the smeared crack approach (for example, Molina et al. [22]). However, the thick walled-cylinder approach introduces some difficulties when extended to real and practical cases, with complex geometry. The smeared crack approach leads to an ill-posed system of equations, localisation instabilities and spurious mesh sensitivity of the FE calculations [23].

The SDA complements the classical approaches, the smeared crack and the discrete crack, and has been successful in the analysis of the fracture of brittle materials. In contrast to the smeared crack model, in the SDA the fracture zone is represented as a discontinuous displacement surface. In contrast to the discrete crack approach, in the SDA the crack geometry is not restricted to interelement lines, as the displacement jumps are embedded in the corresponding finite element displacement field.

This work presents a procedure, based on the SDA, which reproduces the fracture process of concrete around the rebar induced by the expansion of the steel due to corrosion using the cohesive crack approach. The model adopted here [7,8] does not require "crack tracking" to avoid crack locking, as in the case of other works [24,25]. The model has been successful when applied to the fracture of concrete and only requires standard properties of the material, measured by standardised methods.

The results of the proposed models for phases, initiation and propagation, properly fit experimental results.

2. The initiation stage: Development of transport equations

Porous media theories [26] are widely used to describe the thermo-mechanical phenomena related to transport of ions in concrete. The local composition of the mixture ϕ at each geometric point is given by the following expression:

$$\phi^{\alpha} = \frac{dv^{\alpha}}{dv} \tag{1}$$

where $\alpha =$ constituent phase and $v =$ volume.

Adopting as the constituent phases of a partially saturated porous medium microstructure the solid ϕ^s, liquid ϕ^l and gas ϕ^g components, the following condition arises (see Fig. 1):

$$\phi^s + \phi^l + \phi^g = 1. \tag{2}$$

According to Bertolini et al. [27], there are four basic mechanisms concerning the movement of ions and fluids through concrete pores: *capillary suction*, due to surface tension acting in capillaries of cement paste; *permeation*, due to pressure gradients; *diffusion*, due to concentration gradients; and *migration*, due to electrical potential gradients.

The problem of penetration of dissolved agents into concrete is dealt with as an *ideal tracer* problem, which is considered inert with respect to the surrounding media. This is the model used, for example, to describe spreading of pollutants in groundwater [14]. As a first approach to the problem, neglecting the transference of electric charges and the state of stress of the material, two basic mechanisms govern the transport of ions into unsaturated concrete: diffusion and capillary suction (*convection*).

Likewise, cracking is supposed to increase the concrete permeability and acceleration of transport processes. Most researchers related crack width directly to the transport property of the cracked concrete [13]. However, for the sake of simplicity, a sound concrete condition is here assumed in the initiation stage. A dependence of the transport parameters with the crack opening can be incorporated in the model, based on experimental results obtained by other researchers [28], if needed.

In such a way, equations used to reproduce chloride transport in concrete are based on three fundamental variables: *chloride concentration*

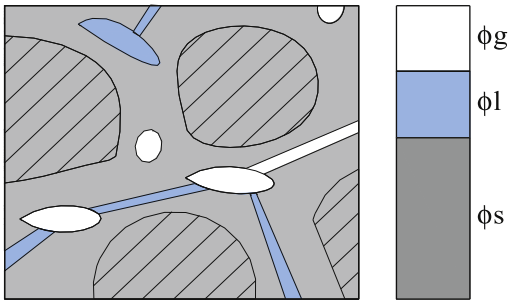

Fig. 1. Semi-saturated porous material phase constituents.

C_c (kg/m^3), *evaporable water content* ω_e (ϕ^l according to Fig. 1) and *temperature T*.

With respect to the first variable, differences between the concentration of *bound chlorides* C_{bc} (kg/m^3 of concrete) and the *free chloride* concentration C_{fc} (kg/m^3 of pore solution) must be distinguished. The *total chloride* concentration C_{tc} (kg/m^3 of concrete) then provides [6]:

$$C_{tc} = C_{bc} + \omega_e C_{fc}. \tag{3}$$

Water is first adsorbed on the surface of capillary pores and then, as the relative humidity increases, water condensates and fills up the pores, starting with the smallest and moving to the larger ones [27]. Consequently, a relation between the pore water content ω_e and the ambient relative humidity h, under equilibrium conditions, can be determined. In the following sections, mathematical expressions based on mass balance, energy conservation and material constitutive equations will be derived.

2.1. Diffusion

In unsaturated concrete, free chloride concentration varies from point to point due to both the different binding ratio of chlorides in concrete and the different water content [10]. Moreover, the process is dependent on electric potential gradients related to the presence of dissolved anions and cations. All these circumstances imply that chloride diffusion in concrete is rather complicated and differs notably from that described by Fick's law, which establishes a flux J_F (kg/m^2/s) proportional to the concentration gradient by means of a coefficient D_F, supposed to be constant:

$$J_F = -D_F \nabla C. \tag{4}$$

However, from a practical point of view, use of the previous equation in a generalised way is accepted in the literature, defining an apparent value of diffusion coefficient D_c or diffusivity:

$$J_d = -\omega_e \left(D_c \nabla C_{fc} \right) \tag{5}$$

where J_d refers to diffusion flux of chloride in concrete per unit area and per unit time (kg/m^2/s) and D_c (m^2/s) is the apparent diffusion coefficient that depends, at least, on concentration, humidity and temperature [6].

2.2. Capillary suction

Models describing moisture diffusion in concrete are usually based on an extension of Darcy's law as a constitutive equation:

$$q_\omega = -K \nabla \omega \tag{6}$$

where q_ω is the flux rate (m/s) and K is the diffusion coefficient (m^2/s) that, for the sake of simplicity, was considered constant in the past. Nevertheless, phenomena of water diffusion in concrete are highly nonlinear [29]. Consequently, this is used again an apparent diffusivity D_h that takes into account humidity, temperature and, also, equivalent hydration time. In addition, the equation is not formulated in terms of water content ω, but relative humidity h (the ratio of the actual amount of water vapour in the concrete pores to the amount when saturated at a given temperature, expressed as a percentage). Thus:

$$q_\omega = -D_h \nabla h. \tag{7}$$

Although the described water transport is due to the capillary potential gradient and consequently not, strictly, a diffusion process, through mass conservation and assuming no chemical reaction between water and solid phase and a constant solution density, the above relationships become:

$$\frac{\partial \omega_e}{\partial t} = div(D_h \nabla h). \tag{8}$$

Likewise, the vaporisation ratio per unit volume in the liquid/gas interface should be considered [15], though here it has been neglected for the sake of simplicity.

2.3. Heat transfer

Temperature T is the third basic variable of the system of equations defined below. Heat transfer is described by means of the first law of thermodynamics, an expression of the principle of conservation of energy, and Fourier's law, with the following well-known equation (in the case of neither heat sources nor soaks):

$$\frac{\partial}{\partial t}(\rho c T) = div(\lambda \nabla T) \tag{9}$$

where ρ is the material density, c is the specific heat and λ the thermal conductivity. Adopting constant values for these three parameters, the resulting equation is linear. Non-linearity of problems related to humidity and chloride concentration comes from the dependence of diffusion coefficients on the abovementioned variables. Although the heat transfer equation is decoupled from the previous equations corresponding to chloride concentration and moisture diffusion, it is worth noting that the different coefficients involved in the system of equations are, in general, highly dependent on temperature.

2.4. Chloride ion transport

On the basis shown in the previous paragraphs, the total free chloride flux in concrete J_{fc} (kg/m^2/s) can be obtained by the addition of the flux due to chloride concentration diffusion and the flux due to convection, that is, ion transport driven by flux of moisture through concrete:

$$J_{fc} = -\omega_e D_c \nabla C_{fc} - C_{fc} D_h \nabla h. \tag{10}$$

Considering a differential element of volume dV, the amount of free chloride that enters the element in a time differential increment dt implies the variation of the total chloride concentration, according to the expression:

$$\frac{\partial C_{tc}}{\partial t} = -div\left(J_{fc} \right). \tag{11}$$

Thus, finally:

$$\left(\frac{\partial C_{bc}}{\partial C_{fc}} + \omega_e \right) \frac{\partial C_{fc}}{\partial t} + C_{fc} \frac{\partial \omega_e}{\partial t} = div\left(\omega_e D_c \nabla C_{fc} \right) + div\left(C_{fc} D_h \nabla h \right). \tag{12}$$

The bound chloride concentration is expressed usually as a function of free chloride concentration in the form of a binding isotherm such as linear, Freundlich or Langmuir (see Fig. 2).

Although chloride binding is not an instantaneous process and one which involves more factors such as the pH of the solution, in actual fact the models from literature use the previous curves in assuming an instantaneous and completely reversible equilibrium between free and bound chlorides.

Chloride binding does not only decrease the total amount of free chlorides in the pore solution, but also reduces considerably their transport velocity [30]. In any case, although only free chloride is directly responsible for the corrosion process, the potential risk due to

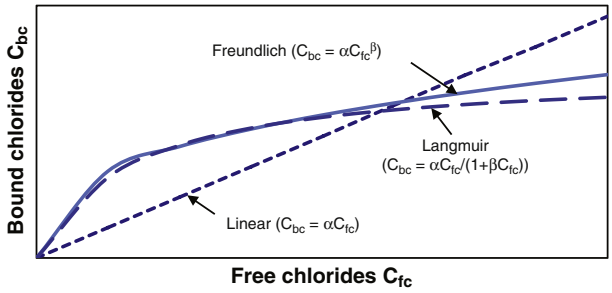

Fig. 2. Chloride binding isotherms.

chloride weakly bound to the solid phase has to be taken into account, in order to establish a concentration threshold.

3. The initiation stage. Finite element formulation

The previous analysis leads to a system of three partial differential equations (Eqs. (8), (9) and (12)) in three variables: free chloride concentration C_{fc}, relative humidity h and temperature T. Moreover, values of C_{bc} (bound chlorides) and ω_e (pore water content) must be known as a function of C_{fc} and h, respectively.

Since the three equations have a similar structure, only the chloride transport case, that is, simplifying Eq. (12), will be developed here:

$$\left(\frac{\partial C_{bc}}{\partial C_{fc}} + \omega_e\right)\frac{\partial C_{fc}}{\partial t} = div\left(\omega_e D_c \nabla C_{fc}\right) + \nabla C_{fc}\cdot D_h \nabla h. \tag{13}$$

Employing Galerkin's method for the finite element formulation, by means of the weight function W, and integrating over the space domain Ω, the following emerges:

$$\int_\Omega W\left(\frac{\partial C_{bc}}{\partial C_{fc}} + \omega_e\right)\frac{\partial C_{fc}}{\partial t}d\Omega = \int_\Omega W\left(div\left(\omega_e D_c \nabla C_{fc}\right) + \nabla C_{fc}\cdot D_h \nabla h\right)d\Omega. \tag{14}$$

Using now Green's theorem, the second-spatial derivatives can be replaced by first derivative terms:

$$\int_\Omega W\left(\frac{\partial C_{bc}}{\partial C_{fc}} + \omega_e\right)\frac{\partial C_{fc}}{\partial t}d\Omega = \oint_{\partial\Omega} W\omega_e D_c \frac{\partial C_{fc}}{\partial n}d\Gamma + \int_\Omega\left(-\nabla W\cdot\omega_e D_c\nabla C_{fc} + W\cdot\nabla C_{fc}\cdot D_h\nabla h\right)d\Omega. \tag{15}$$

The next step is the discretisation of the domain Ω into elemental cells Ω_e. The unknown variables are expressed in terms of the nodal shape functions N_I and the unknown vectors Φ^I, where I is the sub-index referring to the corresponding element node, so that:

$$\phi_{(e)} \cong \sum_{(e)} N_I \phi^I. \tag{16}$$

Using as weight functions the shape functions associated with the element nodes, results:

$$\int_{\Omega e} N_I\left(\frac{\partial C_{bc}}{\partial C_{fc}} + \omega_e\right)\dot{C}_{fc}^J N_J d\Omega_e = \oint_{\partial\Omega e} N_I\omega_e D_c \frac{C_{fc}^J \partial N^J}{\partial n}d\Gamma_e + \int_{\Omega e}\left(-\nabla N_I\cdot\omega_e D_c C_{fc}^J\nabla N_J + N_I C_{fc}^J \nabla N_J\cdot D_h\nabla h\right)d\Omega_e. \tag{17}$$

The previous equation can be expressed in matrix notation:

$$c_{c(e)}\dot{C}_{fc}^{(e)} + k_{c(e)}C_{fc}^{(e)} + f_{c(e)} = 0. \tag{18}$$

The non-linearity of the problem arises from the dependence of capacitance matrix c_c and stiffness matrix k_c on the unknown variables: concentration, humidity and temperature.

For the capacitance matrix, the following arises:

$$c_{c(e)}^{IJ} = \int_{\Omega e} N_I\left(\frac{\partial C_{bc}}{\partial C_{fc}} + \omega_e\right)N_J d\Omega_e \cong \sum_l\left[N_I\left(\frac{\partial C_{bc}}{\partial C_{fc}} + \omega_e\right)N_J\right]_{\xi=l}|J|_{\xi=l}W_{\xi=l}. \tag{19}$$

In Eq. (19), both global (x, y) to local (ξ,η) coordinate transformation and the Gauss–Legendre integration formula have been used, with the corresponding weight factors W_l. Isoparametric formulation was employed.

With respect to the system stiffness matrix:

$$k_{c(e)}^{IJ} = \int_{\Omega e}\left(\nabla N_I(\omega_e D_c)\nabla N_J - N_I(D_h\nabla h)\nabla N_J\right)d\Omega_e \cong \sum_l\left\{\left[\nabla N_I(\omega_e D_c)\nabla N_J\right]_{\xi=l} - \left[N_I(D_h\nabla h)\nabla N_J\right]_{\xi=l}\right\}|J|_{\xi=l}W_{\xi=l}. \tag{20}$$

Finally, the vector of equivalent nodal forces is given by:

$$f_{c(e)}^I = \oint_{\partial\Omega e} N_I (J_d)_n d\Gamma_e. \tag{21}$$

This vector is considered especially in those elements at borders where the diffusion flux J_d is known.

Assembling the elemental matrices in order to cover the whole problem mesh, the well-known expression for a system of linearised first-order differential equation in the time domain, arises:

$$[C_c]\left\{\dot{C}_{fc}\right\} + [K_c]\left\{C_{fc}\right\} = \{F_c\}. \tag{22}$$

In a similar way, humidity and temperature cases can be developed.

Once the system of non-linear equations that governs chloride transport in concrete has been established, as a function of concentration, humidity and temperature variables; a finite element program is necessary to tackle its resolution. Here, the element matrices and vectors needed to assemble the non-linear equation were programmed in a user subroutine in the framework of the Finite Element Analysis Program (FEAP), developed by Taylor [31].

Calculation is based on residual equation for each node i, linearising it in the solving algorithm (Newton method) by means of the tangent matrix S. In the time domain, an implicit finite-difference strategy (Euler method) is used, evaluating the residual at time t_{n+1}, as a function of u_{n+1} values and their derivatives [32].

4. The initiation stage. Model contrast

In order to verify the proposed model, an experimental study carried out by Sergi et al. [33] is simulated. In the experiment, the top surface of a cylindrical hardened OPC paste specimen was exposed to a 1 M NaCl solution meanwhile the other surfaces were insulated.

In essence, the problem to be analysed is a sudden increase in Cl^- concentration in the free surface, accompanied by a change in the ambient relative humidity, under the hypothesis that this sudden increase in the free surface remains constant over time. At the other boundary model edges, a null flux condition is imposed.

The first approximation is based on a simple model through Fick's second law that has an analytical solution for the one-dimensional case of a semi-infinite medium with constant diffusion coefficients (for example, ASTM C 1556-04 [34]):

$$C(x,t) = C_s - (C_s - C_i)\cdot\left[erf\left(\frac{x}{\sqrt{4Dt}}\right)\right] \quad (23)$$

where C represents the chloride concentration, C_s is the surface concentration, C_i the initial value, D is the diffusion coefficient (constant), t the time and x the distance to the free surface.

This is a simple model that takes everything into account by modifying the chloride diffusion coefficient in order to achieve the best fit. This is the reason for the published apparent diffusion coefficient varying from 10^{-10} to 10^{-12} m^2/s [16]. Here the described comprehensive model will be used, taking into account separately aspects such as chloride binding or relative humidity changes, employing an estimation *a priori* of the diffusion coefficient.

Regarding this parameter, the formulae by Martín-Pérez et al. [6] are implemented in the user element, though the influence of equivalent hydration time is not considered here. Consequently:

$$\begin{aligned} D_c &= D_{c,ref} F_1(T) F_3(h) \\ &= D_{c,ref}\ exp\left[\frac{U_c}{R}\left(\frac{1}{T_{ref}} - \frac{1}{T}\right)\right]\left[1 + \frac{(1-h)^4}{(1-h_c)^4}\right]^{-1} \end{aligned} \quad (24)$$

where U_c is the activation energy of the chloride diffusion process, R the gas constant and h_c is the humidity at which D_c drops halfway between its maximum and minimum values ($h_c = 0.75$).

Regarding humidity transport:

$$\begin{aligned} D_h &= D_{h,ref} G_2(T) G_1(h) \\ &= D_{h,ref}\ exp\left[\frac{U_h}{R}\left(\frac{1}{T_{ref}} - \frac{1}{T}\right)\right]\left[0.05 + \frac{0.95}{1 + \left(\frac{1-h}{1-hc}\right)^n}\right] \end{aligned} \quad (25)$$

where n is a parameter characterising the spread of the drop in D_h which takes an average value of 10.

Fig. 3 reproduces the free chloride concentration profile at 100 days. Firstly, experimental data are presented; secondly, the results by the best fit to Fick's equation, with an apparent diffusion coefficient of $1.35\times10^{-}$ m^2/s. Better results are obtained by considering the binding effect through Freundlich isotherm ($\alpha_F = 0.88$; $\beta_F = 0.47$). In this case, the apparent diffusion coefficient is equal to 4.28×10^{-11} m^2 but, again, the analysis *a posteriori* of experimental data appears indispensable.

However, in the present model, an intrinsic diffusion coefficient proposed by Wang et al. [16] that equals 1.02×10^{-10} m^2/s divided by a tortuosity factor ($\tau = 1.9$) squared is used, i.e. 2.825×10^{-11} m^2/s. The influence of a solution convection is clearly shown by comparing results obtained by ignoring the initial humidity of 80% in the samples of the test and considering, then, a saturated condition from the very beginning. For humidity transport, a linear relation between water content and humidity was assumed ($\omega_e = \omega_{sat}\ h$, with ω_{sat} the percentage of water content in saturated material, Saetta et al. [11]) and average parameters from literature adopted for $n = 0.5$, $h_c = 0.75$ and $D_{h,ref} = 5\times10^{-11}$ m^2/s.

The used parameters are summarised in Table 1. In Fig. 4 the free chloride and relative humidity distributions, together with the used finite element mesh, are shown.

Regarding the total chloride profile, a good fit with experimental data (shown in Fig. 5) is obtained. In this case, as was expected, a specific study by Sergi et al. [33] leads to such a best fit. No information is obtained through simple models based exclusively on the second Fick's law.

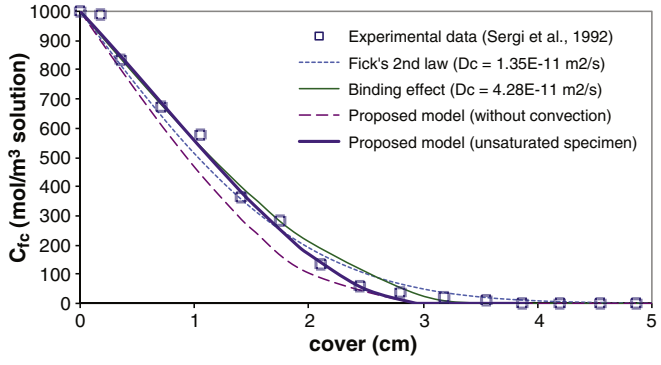

Fig. 3. Free chloride profile after 100 days (refer to tests by Sergi et al. [33]).

5. The propagation stage. Cracking due to rebar corrosion

Once the chloride concentration threshold (for example, Angst et al. [35]) has been reached in the rebar surroundings, the subsequent oxide generation not only implies a steel section reduction, loss of steel ductility [36] and degradation in the steel-concrete adherence, but also increases the total equivalent rebar section. This is so because the volume of the rust products is about four- to six-times higher than that of steel. Consequently, expansive stress appears in the concrete, causing cracking, spalling or delamination of the cover.

Much research has been performed in the last years with respect to this area, some of which involves: Morinaga [37], Andrade et al. [3]; Molina et al. [22], Liu and Weyers [19], Pantazopoulou and Papoulia [38], Bhargava et al. [39,40], and Chernin et al [41]. In spite of the variety of the models, most are based on the hypothesis of a thick-walled cylinder with the wall thickness equal to that of the concrete cover, with different approaches to the non-linear behaviour of concrete after cracking.

Here, a finite element with cohesive embedded crack [7–9], based on the SDA approach will be used. This embedded crack element does not need a crack tracking algorithm. As the cracking pattern caused by corrosion phenomena includes multiple cracks and branching, this feature of the used formulation is of special relevance. The plane model avoids the classical central symmetry condition with respect to the bar axis with a contact algorithm employed to reproduce the oxide–concrete interface. Before describing the proposed model, some aspects about cohesive embedded crack will be outlined below.

6. Finite element with cohesive embedded crack

Consider a conventional finite element like that shown in Fig. 6, with a straight crack inside. The element is split in two sub-domains, separated by a displacement jump **w**.

Table 1
Initiation stage. Parameters and initial data of specimen.

Parameter	Symbol	Value	Unit
Reference temperature	T_{ref}	20	°C
Activation energy of the chloride diffusion	U_c	44.600	kJ/mol
Chloride diffusion coefficient	$D_{c,ref}$	2.825E-11	m^2/s
Freundlich α binding constant	α_F	0.88	
Freundlich β binding constant	β_F	0.47	
Activation energy of hydration	U_h	30.762	kJ/mol
Humidity diffusion coefficient	$D_{h,ref}$	5.E-11	m^2/s
Parameter n	n	10	
Parameter h_c	h_c	0.75	
Evaporable water content in saturated concrete	ω_{sat}	0.11	
Ratio g water/g cement	–	0.3	

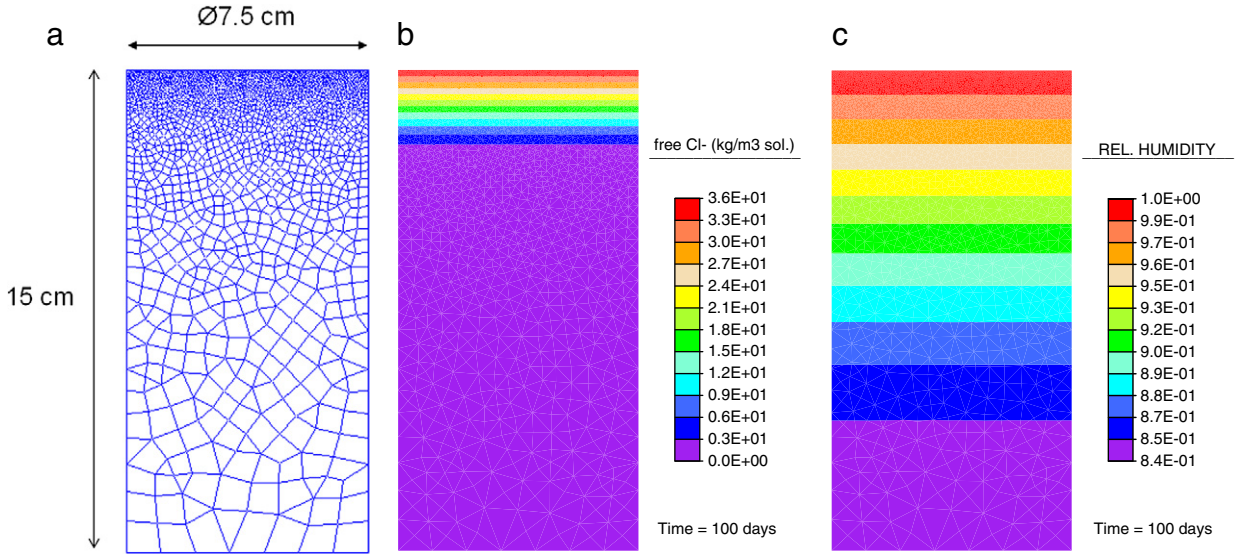

Fig. 4. Initiation stage. Proposed model results: (a) FEM model; (b) free chloride profile; and (c). Relative humidity.

According to the strong discontinuity approach (for example, Oliver [24]), the approximated displacement field within the element can be written as:

$$\boldsymbol{u}(x) = \sum_{(A)} N_1(x)\boldsymbol{u}^1 + \left[H(x) - N^+(x)\right]\boldsymbol{w} \tag{26}$$

where $N_I(x)$ is the traditional shape function for node I, $\boldsymbol{u}^I$ the corresponding nodal displacement and $H(x)$ the Heaviside jump function across the crack plane. Moreover,

$$N^+(x) = \sum_{(1\in A^+)} N_1(x). \tag{27}$$

The strain tensor is obtained from the displacement field as a continuous part plus a Dirac's δ function on the crack line. The continuous part is given by:

$$\boldsymbol{\varepsilon}^c(x) = \boldsymbol{\varepsilon}^a(x) - \left[\boldsymbol{b}^+(x)\otimes\boldsymbol{w}\right]^s \tag{28}$$

where $\boldsymbol{\varepsilon}^a$ (the apparent strain tensor) and $\boldsymbol{b}^+$ are obtained as follows:

$$\begin{aligned}\boldsymbol{\varepsilon}^a(x) &= \sum_{(A)} \left[\boldsymbol{b}_1(x)\otimes\boldsymbol{u}^I\right]^s \\ \boldsymbol{b}^+(x) &= \sum_{(A^+)} \boldsymbol{b}_1(x)\end{aligned} \tag{29}$$

with $\boldsymbol{b}_I(x) = \mathbf{grad}\ N_I(x)$ and superscript ^{S} indicating symmetric part of a tensor.

A simple generalisation of the cohesive crack to mixed mode is used, one which assumes that the traction vector $\boldsymbol{t}$ transmitted across the crack faces is parallel to the crack displacement vector $\boldsymbol{w}$ (central forces model). To cope with the possibility of unloading [7,8]:

$$\boldsymbol{t} = \frac{f(\tilde{w})}{\tilde{w}}\boldsymbol{w} \tag{30}$$

where $f(\tilde{w})$ is the classical softening function for pure opening mode (Fig. 7) and $\tilde{w}$ is an equivalent crack opening defined as the historical maximum of the magnitude of the crack displacement vector.

Outside the crack line, an elastic and linear behaviour is assumed. The stress tensor is given, from Eqs. (28) to (30):

$$\sigma = \mathbf{E}:\left[\boldsymbol{\varepsilon}^a - \left(\mathbf{b}^+\otimes\mathbf{w}^s\right)\right] \tag{31}$$

$$\frac{f(\tilde{w})}{\tilde{w}}\boldsymbol{w} = \mathbf{E}:\left[\boldsymbol{\varepsilon}^a - \left(\boldsymbol{b}^+\otimes\boldsymbol{w}\right)^s\right]\cdot\boldsymbol{n}. \tag{32}$$

Developing the former expression, finally:

$$\left[\frac{f(\tilde{w})}{\tilde{w}}1 + \boldsymbol{n}\cdot\mathbf{E}\cdot\boldsymbol{b}^+\right]\cdot\boldsymbol{w} = \left[\mathbf{E}:\boldsymbol{\varepsilon}^a\right]\cdot\boldsymbol{n}. \tag{33}$$

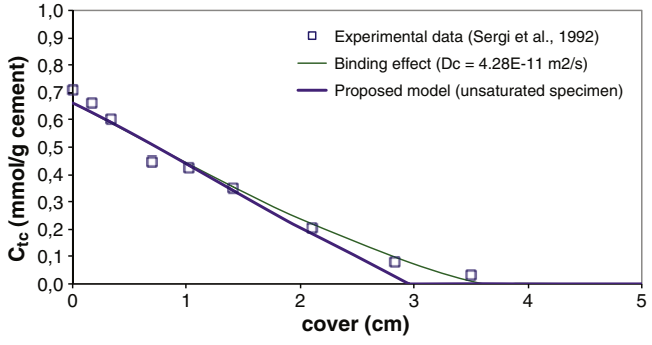

Fig. 5. Total chloride profile after 100 days (refer to tests by Sergi et al. [33]).

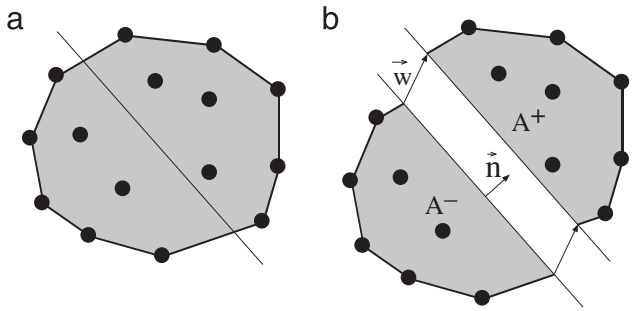

Fig. 6. Finite element with an embedded crack: (a) generic element with nodes and crack line; and (b) displacement jump across the crack line.

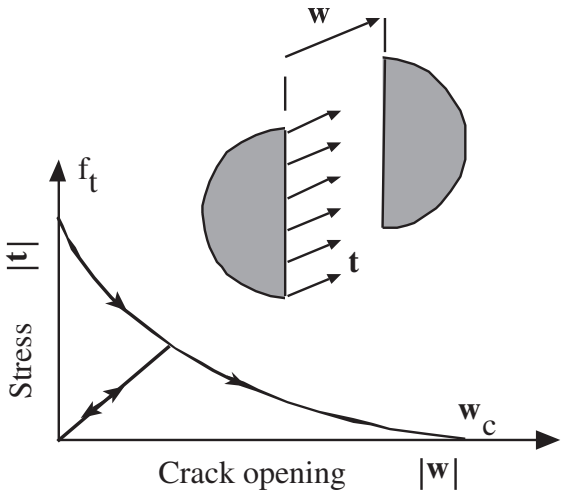

Fig. 7. Sketch of the softening curve for the cohesive crack model.

Table 2
Propagation stage. Experimental data of slab specimen L1 [43].

Parameter	Symbol	Value	Unit
Initial rebar diameter	D_i	16	mm
Clear cover to the reinforcement	c	48	mm
Rebar spacing	s	200	mm
Annual mean corrosion rate	i_{corr}	2.41	μA/cm^2
Compressive strength of concrete	f_c	31.5	MPa
Modulus of elasticity of cover concrete	E_c	27,000	MPa
Tensile strength of concrete	f_{ct}	3.3	MPa
Poisson's ratio of concrete	ν_c	0.18	
Creep coefficient for the concrete cover	φ	2.0	
Thickness of porous zone around steel–concrete interface	d_o	0.0125	mm

This equation is solved for $\boldsymbol{w}$ using Newton Raphson's method, given the nodal displacements (and so $\boldsymbol{\varepsilon}^a$) once the crack is formed and thus $\boldsymbol{n}$ and $\boldsymbol{b}^+$ are also known. Regarding crack initiation, for CST triangles, a node is selected so that the side opposite to it is as parallel as possible to the crack [7,8,42].

Finally, to avoid locking after a certain crack growth, some degree of crack adaptability within each element is implemented, allowing the crack to adapt itself to the later variations in the principal stress direction while its opening is small. Threshold values must be related to the softening properties of the material. Values around 0.1–0.2 G_F/f_t are usually satisfactory [7,8]. Above these threshold values, the crack is considered consolidated.

7. The propagation stage. Application example

Once again, the numerical model should be contrasted with experimental results. On this occasion, the reference is the slab specimen L1 subjected to accelerated corrosion tests developed by Liu [43]. Table 2 summarises the main experimental data and Fig. 8 sketches the geometry of the problem.

For the sake of simplicity, the mechanical properties of oxide products are adopted as the steel ones, in accordance with the assumption offered by Bhargava and Ghosh [21]. The FE model is represented in Fig. 9, with a characteristic element length in the steel-concrete interface of 0.1 mm. As mentioned earlier, a contact element in the steel (oxide)–concrete interface is necessary to localise cracking and avoid tensile stress in the reinforcement bar [5]. A perfect sliding contact was chosen here.

Oxide production is modelled as an increment of area in the rebar section, as usually adopted in the literature. The initial radius of steel bar R_i is reduced to R_i^*, while corrosion products would reach a radius $R_i + \Delta$ if not constrained by concrete (see Fig. 10). Uniform corrosion around the bar is, then, considered. In addition, the plane strain condition is considered, as well as the exponential function for a softening curve with an estimated value of $G_F = 100$ N/m.

Loss of steel mass j_s is related to the amount of current i_{cor} using Faraday's law:

$$j_s = \frac{M_{Fe}\, i_{cor}}{nF} \tag{34}$$

where M_{FE} is the atomic weight of iron (55.9 g/mol), n the valence of the reaction (typically, $n = 2$ or 3. A weighted average value of $n = 2.5$ will be assumed here) and F the Faraday's constant (96,500 °C/mol).

The amount of steel per unit length of the reinforcement being consumed by the corrosion process W_s is given by:

$$W_s = \rho_s \frac{\pi}{4}\left(D_i^2 - D_i^{*2}\right). \tag{35}$$

It is necessary to define the ratio of volume of expansive corrosion products to the volume of steel consumed μ_v:

$$\mu_v = \frac{(D_i + 2\Delta)^2 - D_i^{*2}}{D_i^2 - D_i^{*2}}. \tag{36}$$

Developing the former expressions, the following emerges:

$$t(\Delta) = \frac{W_s}{\pi D_i j_s} = \frac{\rho_s}{4 D_i j_s (\mu_v - 1)}\left[(D_i + 2\Delta)^2 - D_i^2\right]. \tag{37}$$

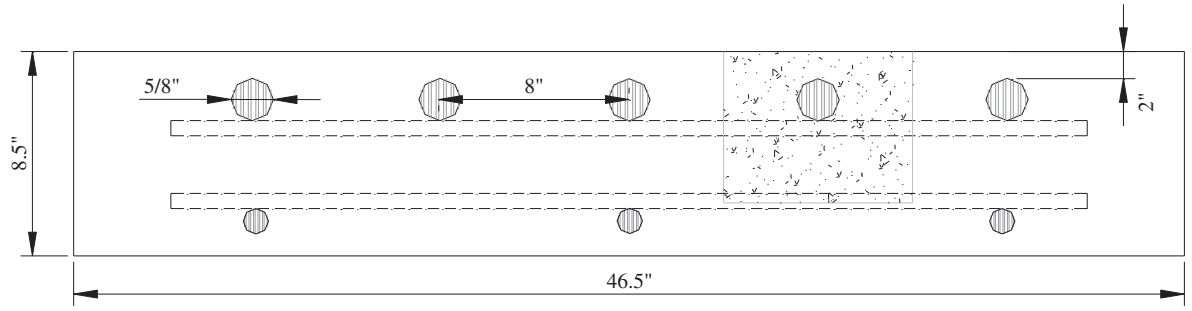

Fig. 8. Sketch of slab specimen L1 [43].

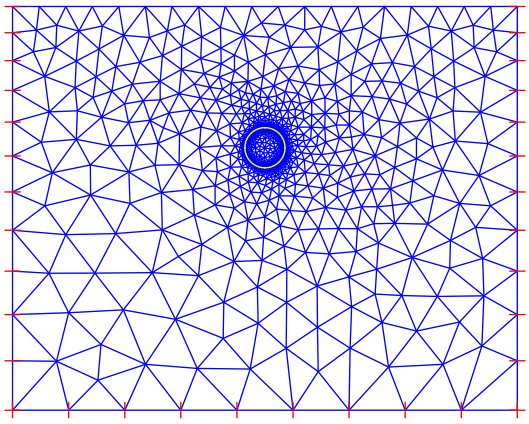

Fig. 9. FE model of slab specimen L1 [43].

Once the ratio of molecular weight of iron to the molecular weight of the corrosion products μ_w is known, the density of rust can be evaluated through the following expression:

$$\rho_r = \frac{\rho_s}{\mu_w \mu_v}. \tag{38}$$

In this work, $\mu_w = 0.613$ and $\mu_v = 3.39$ [40], were assumed. For a steel density of 7860 kg/m^3 the rust density is 3780 kg/m^3.

Additionally, a porous zone (in fact, an especially porous zone) around the bar is considered, taking into account that corrosion products accumulating around the reinforcement bar do not exert any pressure on the surrounding concrete until they fully fill voids between steel and concrete. According to Liu and Weyers [19] this porous thickness is equal to 12.5 μm, which implies an increment in time to cracking around 90 days, by substituting in the expression:

$$t(\Delta = d_0) \simeq \frac{\rho_s d_0}{j_s(\mu_v - 1)}. \tag{39}$$

Table 3 reproduces the relation between time (years) and radius increment Δ (%); and Fig. 11 the corresponding crack pattern for each such time.

Estimation of time to cracking is slightly lower than the experimental ones (1.84 years, according to Liu [43]). However, it must be taken into account that no amount of corrosion products has been accommodated within the open cracks during the progress of cracking. In fact, steel losses indicated in Table 3 do not reach the experimental value of 0.393 mg/mm^2. If only the volume of consolidated cracks with width >0.1 mm in Fig. 11(d) approximately 4 mm^2 (i.e. rust amount of 0.0154 kg/m) is considered; an additional time to cracking of 1.07 years corresponds. In such away, experimental values are tallied.

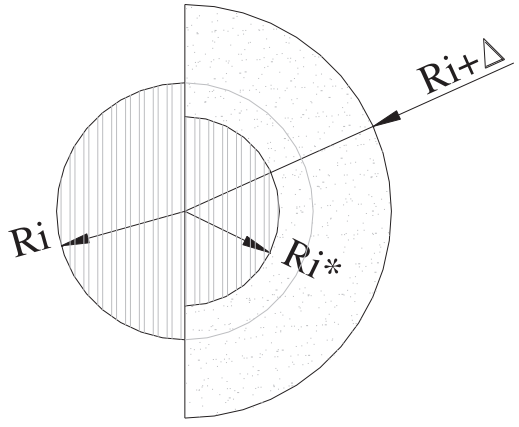

Fig. 10. Reinforcement bar oxidation process sketch.

Table 3
Correspondence between times and radial expansion due to rust production, in slab specimen L1 [43].

Δ (%)	D_o (m)	D_2 (m)	W_r (kg/m)	W_r (d_o) (kg/m)	$W_s + W_s$ (d_o) (kg/m^2)	t (year)
0.20	0.016	0.016032	0.004394	0.003432	0.095	0.54
0.40	0.016	0.016064	0.008797	0.003432	0.149	0.85
0.60	0.016	0.016096	0.013209	0.003432	0.203	1.15
0.80	0.016	0.016128	0.017630	0.003432	0.257	1.46

Although the estimated time to cracking is somewhat conservative; the crack patterns obtained adequately reproduce those observed in the experiments. While vertical cracks do appear on the surface, as the corrosion process progresses cracks tend to localise on the horizontal plane between the reinforcement bars, as predicted by others (for example, Chen [13]). Whereas the opening width of the surface crack in Fig. 11(d) is approximately 0.05 mm, the horizontal one reaches a value greater than 0.1 mm in the surroundings of the reinforcement bar.

8. Conclusions

This work deals jointly with the two phases widely adopted in the literature concerning cover cracking of concrete due to rebar corrosion induced by chloride penetration: the initiation stage and the propagation stage. These phases have been traditionally analysed separately. In this paper, the models for both phases are incorporated in the same finite element program. The models are chained, though not explicitly coupled, as a first step towards their future full integration.

Concerning the initiation stage, the proposed finite element model reproduces results of experimental tests [33] by means of *a priori* parameter estimations, according to the characteristics of materials and external environment conditions. The introduction of hygrometric conditions and convection phenomena appears to be of high significance. However, electrostatic interaction among ions was neglected and sound concrete condition was assumed. A one-dimensional problem was simulated, though the proposed model can also reproduce bi-dimensional complex geometries, for example, cracked concrete cover, as well as variable surface condition.

Concerning the propagation stage, once some conceptual difficulties concerning the localisation of cracks were solved, the proposed model, based on an embedded cohesive crack element, developed by Sancho et al. [7,8], is able to estimate time to surface cracking quite accurately (according to tests by Liu [43]). However, it is necessary to make some assumptions about the consideration of an especially porous zone around the steel–concrete interface and the accommodation of corrosion products within the open cracks generated in the process. In addition, the rust mechanical properties need further analysis. FE geometry avoids axysimmetric conditions and introduces a contact algorithm in the concrete–steel (rust) interface. The crack patterns obtained agree well with expectation.

Despite the adopted simplifications, the present study contributes substantially to the ultimate objective of obtaining a computational framework to assess quantitatively the long-term durability of reinforced concrete structures subjected to chloride attack. Complete integration of the two models and the introduction of items such as material heterogeneity and rust specific properties are objectives of future work.

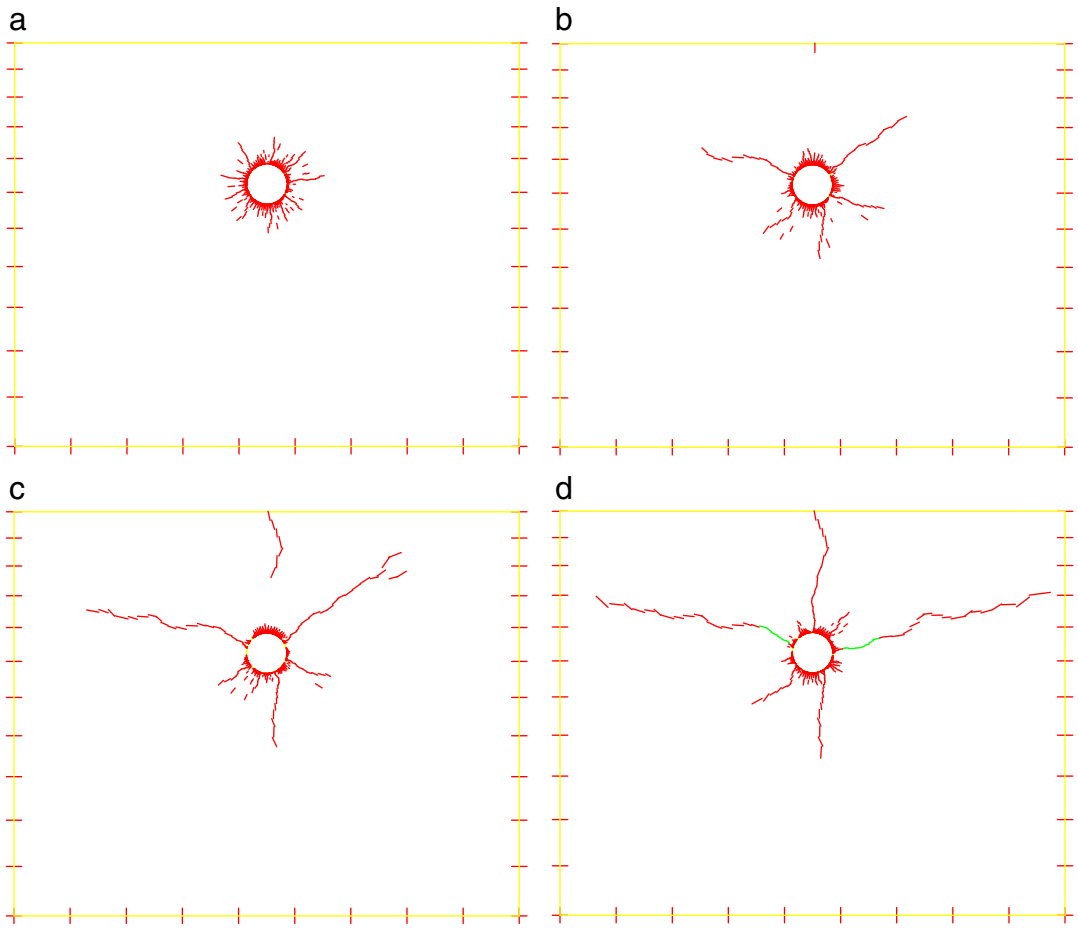

Fig. 11. Propagation stage. Crack pattern in slab specimen L1 (in green, consolidated cracks with width >0.1 mm): (a) 0.54 years; (b) 0.85 years; (c) 1.15 years; and(d) 1.46 years.

References

[1] T.J. Kirkpatrick, R.E. Weyers, C.M. Anderson-Cook, M. Sprinkle, Probabilistic model for the chloride-induced corrosion service life of bridge decks, Cement and Concrete Research 32 (2002) 1943–1960.

[2] K. Tuutti, Corrosion of Steel in Concrete, Swedish Cement and Concrete Research Institute, Stockholm, 1982.

[3] C. Andrade, C. Alonso, F.J. Molina, Cover cracking as a function of bar corrosion: part 1 — experimental test, Materials and Structures 26 (1993) 453–464.

[4] M. Castellote, C. Andrade, Round-robin test on methods for determining chloride transport parameters in concrete, Materials and Structures 39 (2006) 955–990.

[5] Guzmán, S. 2010. Modelización del deterioro de tableros de puentes de hormigón por difusión de cloruros y corrosión de la armadura pasiva. Ph.D. dissertation, Universidad Politécnica de Madrid, Spain. (in Spanish).

[6] B. Martín-Pérez, S.J. Pantazopoulou, M.D.A. Thomas, Numerical solution of mass transport equations in concrete structures, Computers and Structures 79 (2001) 1251–1264.

[7] J.M. Sancho, J. Planas, J.C. Gálvez, E. Reyes, D.A. Cendón, An embedded crack model for finite element analysis of mixed mode fracture of concrete, Fatigue Fract. Engng. Mater Struct 29 (2006) 1056–1065.

[8] J.M. Sancho, J. Planas, D.A. Cendón, E. Reyes, J.C. Gálvez, An embedded crack model for finite element analysis of concrete fracture, Engineering Fracture Mechanics 74 (2007) 75–86.

[9] J.M. Sancho, J. Planas, A.M. Fathy, J.C. Gálvez, D.A. Cendón, Three-dimensional simulation of concrete fracture using embedded crack elements without enforcing crack path continuity, International Journal for Numerical and Analytical Methods in Geomechanics 31 (2007) 173–187.

[10] M. Nagesh, B. Bishwajit, Modeling of chloride diffusion in concrete and determination of diffusion coefficients, ACI Materials Journal 95 (2) (1998).

[11] A.V. Saetta, R.V. Scotta, R.V. Vitaliani, Analysis of chloride diffusion into partially saturated concrete, ACI Materials Journal 90 (5) (1993).

[12] M. Masi, D. Colella, G. Radaelli, L. Bertolini, Simulation of chloride penetration in cement-based materials, Cement and Concrete Research 27 (1997) 1591–1601.

[13] Chen, D. 2006. Computational framework for durability assessment of reinforced concrete structures under coupled deterioration processes. Ph.D. dissertation, Vanderbilt University, Nashville, Tennessee.

[14] B.F. Johannesson, Non linear transient phenomena in porous media with special regard to concrete and durability, Advanced Cement Based Material 6 (1997) 71–75.

[15] E. Samson, J. Marchand, K.A. Snyder, J.J. Beaudoin, Modeling ion and fluid transport in unsaturated cement systems in isothermal conditions, Cement and Concrete Research 35 (2005) 141–153.

[16] Y. Wang, L. Li, C.L. Page, Modelling of chloride ingress into concrete from a saline environment, Building and environment 40 (12) (2005) 1573–1582.

[17] R. Cigna, E. Proverbio, G. Rocchini, A study of reinforcement behaviour in concrete structures using electrochemical techniques, Corrosion Science 35 (5–8) (1993) 1579–1584.

[18] K. Suda, S. Misra, K. Motohashi, Corrosion products of reinforcing bars embedded in concrete, Corrosion Science 35 (5–8) (1993) 1543–1549.

[19] Y. Liu, R. Weyers, Modeling the time-to-corrosion cracking in chloride contaminated reinforced concrete structures, ACI Materials Journal 95 (6) (1998) 675–681.

[20] J.C. Simó, X. Oliver, F. Armero, An analysis of strong discontinuities induced by strain-softening in rate-independent inelastic solids, Computational Mechanics 12 (1993) 277–296.

[21] K. Bhargava, A.K. Ghosh, Analytical model of corrosion-induced cracking of concrete considering the stiffness of reinforcement, Structural Engineering and Mechanics 16 (2003) 749–769.

[22] F.J. Molina, C. Alonso, C. Andrade, Cover cracking as a function of rebar corrosion: part 2 — numerical model, Materials and Structures 26 (1993) 532–548.

[23] Z.P. Bažant, J. Planas, Fracture and Size Effect in Concrete and Other Quasibrittle Materials, CRC Press, New York, 1998.

[24] X. Oliver, Modelling strong discontinuities in solid mechanics via strain softening constitutive equations. Part 1: fundamentals, International Journal for Numerical Methods in Engineering 39 (1996) 3575–3600.

[25] P.J. Sánchez, A.E. Huespe, J. Oliver, S. Toro, Mesoscopic model to simulate the mechanical behavior of reinforced concrete members affected by corrosion, International Journal of Solids and Structures 47 (2010) 559–570.

[26] F. Bangert, D. Kuhl, G. Meschke, Chemo-hygro-mechanical modelling and numerical simulation of concrete deterioration caused by alkali-silica reaction, International Journal for Numerical and Analytical Methods in Geomechanics 28 (2004) 689–714.

[27] L. Bertolini, B. Elsener, P. Pedeferri, R.P. Polder, Corrosion of Steel in Concrete, WILEY-VCH Verlag GmbH & Co, KGaA, Weinheim, 2004.

[28] M. Ismail, A. Toumi, R. François, R. Gagné, Effect of a crack opening on the local diffusion of chloride in cracked mortar samples, Cement and Concrete Research 38 (2008) 1106–1111.
[29] Z.P. Bažant, L.J. Najjar, Nonlinear water diffusion in nonsaturated concrete, Materials and Structures 5 (25) (1972).
[30] B. Martín-Pérez, H. Zibara, R.D. Hooton, M.D.A. Thomas, A study of the effect of chloride binding on service life predictions, Cement and Concrete Research 30 (2000) 1215–1223.
[31] R.L. Taylor, FEAP — A Finite Element Analysis Program, Version 7.5 Programmer Manual, 2005.
[32] O.C. Zienkiewicz, R.L. Taylor, J.H. Zhu, The Finite Element Method, Elsevier and CIMNE, Barcelona, 2006.
[33] G. Sergi, S.W. Yu, C.L. Page, Diffusion of chloride and hydroxyl ions in cementitious materials exposed to a saline environment, Concrete Research 44 (1992) 63–69.
[34] ASTM International: C 1556–04. Standard Test Method for Determining the Apparent Chloride Diffusion Coefficient of Cementitious Mixtures by Bulk Diffusion, 2004.
[35] U. Angst, B. Elsener, C.K. Larsen, Ø. Vennesland, Critical chloride content in reinforced concrete — a review, Cement and Concrete Research 39 (2009) 1122–1138.
[36] Y.G. Du, A.H. Clark, A.H.C. Chan, Effect of corrosion on ductility of reinforcing bars, Magazine of Concrete Research 57 (7) (2005) 407–419.
[37] S. Morinaga, Prediction of service lives of reinforced concrete buildings based on rate of corrosion of reinforcement steel, Special Report of Institute of Technology Shimizu Corporation, Japan. 1988, p. 23.
[38] S.J. Pantazopoulou, K.D. Papoulia, Modeling cover-cracking due to reinforcement corrosion in RC structures, Journal of Engineering Mechanics 127 (4) (2001).
[39] K. Bhargava, A.K. Ghosh, Y. Mori, S. Ramanujam, Modeling of time to corrosion-induced cover cracking in reinforced concrete structures, Cement and Concrete Research 35 (2005) 2203–2218.
[40] K. Bhargava, A.K. Ghosh, Y. Mori, S. Ramanujam, Analytical model for time to cover cracking in RC structures due to rebar corrosion, Nuclear Engineering and Design 236 (2006) 1123–1139.
[41] L. Chernin, D.V. Val, K.Y. Volkh, Analytical modelling of concrete cover cracking caused by corrosion of reinforcement, Materials and Structures 43 (4) (2010) 543–556.
[42] R.I. Borja, A finite element model for strain localization analysis of strongly discontinuous fields based on standard Galerkin approximation, Computer Methods in Applied Mechanics and Engineering 190 (2000) 1529–1549.
[43] Liu, Y. 1996. Modeling the Time-to-Corrosion Cracking of the Cover Concrete in Chloride Contaminated Reinforced Concrete Structures. Ph.D. dissertation, Virginia Polytechnic Institute and State University, Blacksburg, Va.
[44] R. Barbarulo, J. Marchand, K.A. Snyder, S. Prené, Dimensional analysis of ionic transport problems in hydrated cement systems. Part I: Theorical considerations. Cement and Concrete Research 30 (12) (2000) 1955–1960.